D 3   Chirality in the motion of microswimmers: from circle swimmers to bacterial turbulence

H. Löwen

Institut für Theoretische Physik II: Weiche Materie

Heinrich-Heine Universität Düsseldorf

Contents

1　Abstract

In these notes, we summarize recent progress in our understanding of the basic physical principles of microswimmers which perform a motion characterized by chirality. We discuss both the chiral motion of single circle swimmer and the occurrence of bacterial turbulence where swirls of different chirality are formed spontaneously in an ensemble of linear microswimmers. Some recent highlights in this context as obtained by theory, simulation and experiment are summarized and briefly discussed.

2　Introduction

This article briefly summarizes and reviews two aspects of chiral motion of microswimmers, namely the chiral motion of single circle swimmers and the occurrence of a new turbulent swirling state in self-propelled rod systems and dense bacterial suspensions. We intend to focus on the essential physics and do not give a comprehensive review. Rather we describe recent developments and try to explain them in a brief and concise way.

3　Chirality in circle swimming

3.1　Active Brownian motion with chirality (circle swimming)

Swimming along a straight line (corresponding to linearly directed Brownian motion) is the exception rather than the rule. Ideal straight swimming only occurs if the left-right symmetry relative to the internal propulsion direction is not broken. A linear trajectory is getting unstable with respect to small deviations from this symmetry exhibiting a *chirality*. In two spatial dimensions, this will result in circle-swimming, in three dimensions, correspondingly, there is swimming along a helical path ("helical swimming"). Clearly one can assign a chirality (or helicity) to the path, the sign of which determines whether the motion is clockwise or anti-clockwise.

The occurence of spiral-like swimming motions of microorganisms was pointed out more than a century ago by Jennings [1] and since then was found in many different situations, in particular close to a substrate where certain bacteria [2–7] and spermatozoa [8–10] swim in circles. Likewise helical motion was observed for different bacteria and sperm cells [1, 11–18]. Examples for non-living but active particles moving in circles are spherical camphors at an air–water interface [19] and chiral colloidal swimmers on a substrate [20]. The latter have provided excellent model systems to test the basic assumptions of chiral active Brownian motion. Finally, trajectories of deformable active particles [21] and even of completely blinded and ear-plugged pedestrians [22] can possess significant circular characteristics.

The origin of chiral motion can be manifold. The most obvious is an anisotropy in the particle shape which leads to a translation-rotation coupling in the hydrodynamic sense [23]. But also an anisotropy in the propulsion mechanism itself leads to chiral motion. An example where both mechanisms are simultaneously is presented in figure 1 where trajectories of two L-shape swimmers with different chiralities are shown. A cluster of linear swimmers which sticks together by direct forces [24] or hydrodynamics or just by the activity itself [25] will in general lead to a situation where the total torque acting on the cluster center is not vanishing [26]. This
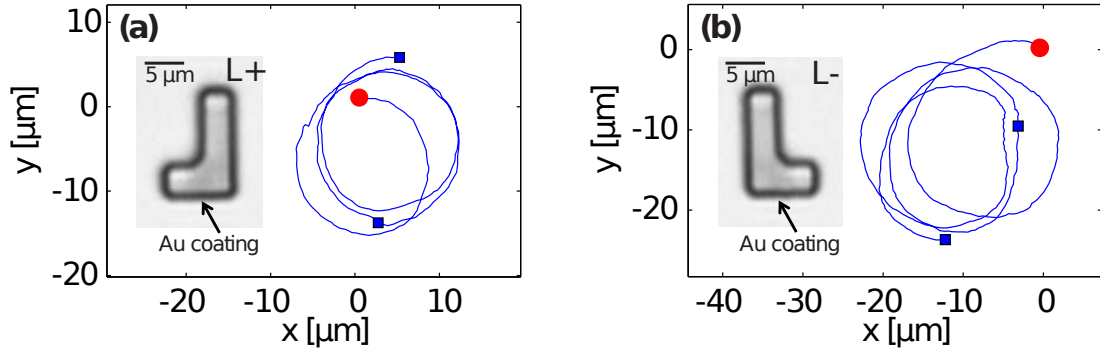
Fig. 1: *Trajectories of an (a) L^+ and (b) L^- swimmer driven by self-diffusiophoresis, (Red) bullets and (blue) square symbols correspond to initial particle positions and those after 1 min each, respectively. The insets show microscope images of two different swimmers with the Au coating (not visible in the bright-field image) indicated by an arrow. From Ref. [20].*

leads to circling clusters. Finally the particle rotation can be induced by external fields, a standard example is a magnetic field perpendicular to the plane of motion which will exert a torque on the particles [27].

The equations of motion for chiral swimming can easily be understood in two spatial dimensions. Consider a polar particles as described by a center-of-mass coordinate $\vec{r}$ and a unit orientation vector $\hat{u}$ which has a relative orientation with respect to the x-axis as given by the angle ϕ such that $\hat{u} = (\cos\phi, \sin\phi)$, see figure 1 for a schematic illustration. We consider overdamped Brownian motion for both translational and orientational degrees of freedom and introduce a systematic drift in the orientation as mediated by a constant torque M in the direction perpendicular to the plane of motion. The equations of motion therefore are

$$\dot{\vec{r}} = \beta \overleftrightarrow{D} \left(F\hat{u} - \vec{\nabla}V\left(\vec{r}, \phi\right) + \vec{f} \right) \tag{1}$$

$$\dot{\phi} = \beta D_r \left(M - \partial_\phi V\left(\vec{r}, \phi\right) + \tau \right) \tag{2}$$

Here, $V(\vec{r}, \phi)$ is an external one-body potential that can be set to zero, $\vec{f}$ and τ are Gaussian distributed random numbers characterizing the Brownian noise for the translation and rotation. Their first moment is vanishing and the second moment is related to an (effective) system temperature T (with $\beta = 1/k_B T$).

Finally F is an effective self-propulsion force directed along the particle orientation which is proportional to the swimming speed. The term βD_r is an inverse rotational friction coefficient, or D_r is a rotational diffusion coefficient while the translational diffusion tensor is given by

$$\overleftrightarrow{D} = D_\parallel \hat{u} \otimes \hat{u} + D_\perp \left(\overleftrightarrow{I} - \hat{u} \otimes \hat{u} \right) \tag{3}$$

with two translational diffusion constants perpendicular and parallel to the orientation.

Let us discuss the solution of these equations in the bulk when $V(\vec{r}, \phi)$ is vanishing. In the noise free case ($\vec{f} = 0$ and $\tau = 0$) the deterministic solution of the equations of motion (1) and (2) are closed circles, see figure 3. The circle radius is given by

$$R_0 = \frac{D_\parallel F}{D_r M} \tag{4}$$

and the spinning frequency ω is

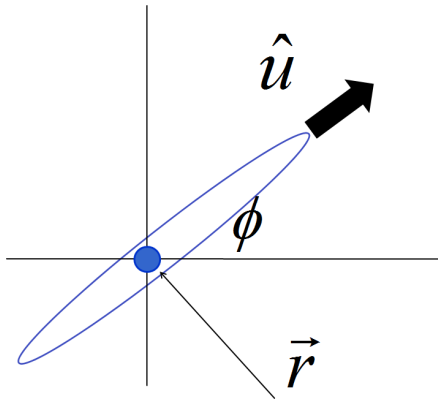$$\omega = \beta D_r M \tag{5}$$

Fig. 2: *Sketch of the orientation $\hat{u}$ and position $\vec{r}$ of an active rod.*
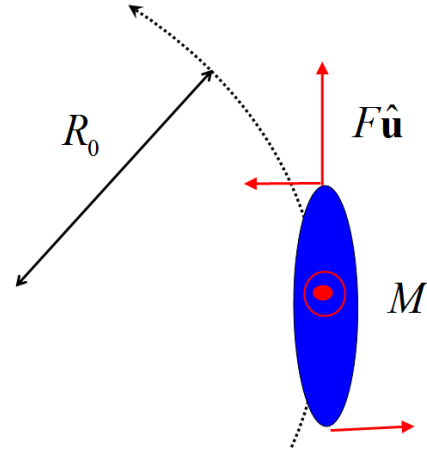

Fig. 3: *Trajectory of a circle swimmer and direction of the self-propulsion force $F\hat{u}$ and torque M.*
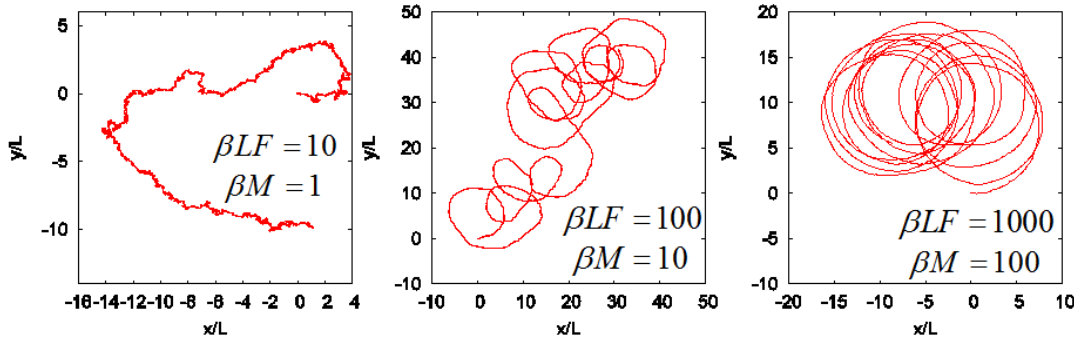

Fig. 4: *Typical Brownian dynamics simulation results for the trajectory of a circle swimmer. The different snapshots are for three different noise strengths.*

For finite noise, there are three regimes: for very short times the motion is diffusive, then there is a crossover towards a (albeit curved) ballistic regime and then for very long times there is again diffusion. Examples for circle-swimming particle trajectories are presented in figure 4 at three different strengths of noise. The first two noise-average moments of the circle swimmer can be computed analytically [28] generalizing the seminal result of Howse et al for linear swimmers [29] as a generalization for active Brownian linear swimming where now the orientational degrees of freedom experience a systematic drift which can be described by an effective torque. One obtains

$$\overline{\vec{r} - \vec{r}(0)} = \lambda \left[D_r \hat{u}_0^\perp - e^{-D_r t} \left(D_r \bar{\hat{u}} + \omega \bar{\hat{u}}^\perp \right) \right] \tag{6}$$

$$\overline{(\vec{r} - \vec{r}(0))^2} = 2\lambda^2 \Big\{ \omega^2 - D_r^2 + D_r \left(D_r^2 + \omega^2 \right) t$$

$$+ e^{-D_r t} \left[\left(D_r^2 - \omega^2 \right) \cos(\omega t) - 2 D_r \omega \sin(\omega t) \right] \Big\} + 2 \left(D_\parallel + D_\perp \right) t \tag{7}$$

where the overbar denotes a noise-average, λ is defined as

$$\lambda = \beta D_\parallel F / \left(D_r^2 + \omega^2 \right) \tag{8}$$

$\hat{u}(0) = (\cos\phi_0, \sin\phi_0)$ is the initial orientation and $\vec{r}(0)$ the initial position. Moreover

$$\hat{u}_0^\perp = (-\sin\phi_0,\ \cos\phi_0) \tag{9}$$

$$\overline{\hat{u}} = (\cos\bar{\phi},\ \sin\bar{\phi}) \tag{10}$$

$$\overline{\hat{u}^\perp} = (-\sin\bar{\phi},\ \cos\bar{\phi}) \tag{11}$$

where $\bar{\phi}$ is the noise average over the angles given by

$$\bar{\phi} = \phi_0 + \omega t\,. \tag{12}$$

For a linear swimmer the first moment simplifies to

$$\langle \vec{r}(t)\rangle = \vec{r}(0) + \hat{u}(0)\frac{v_0}{D_r}(1 - \exp(-D_r t)) \tag{13}$$

where v_0 is the self-propulsion speed. So for given initial position and orientation it is a piece of a straight line directed along the initial orientation. Interestingly the swimmer on average does not proceed to infinity but only recovers a characteristic persistence length which is given by $\ell_p = v_0/D_r$.

Discussing the first moment (6) for chiral swimmers is more complicated. The mean trajectory is now generalized to a *spira mirabilis* or a logarithmic spiral. By eliminating the time t one obtains in polar coordinates the following representation for the trajectory in coordinates:

$$r(\phi) \propto \exp(-D_r(\phi - \phi_0)/\omega) \tag{14}$$

where $\hat{u}(0) = (\cos\phi_0, \sin\phi_0)$ and ω is the characteristic circling frequency. Recent experiments on chiral colloidal microswimmers have confirmed this prediction [20] as documented in Figure 5.
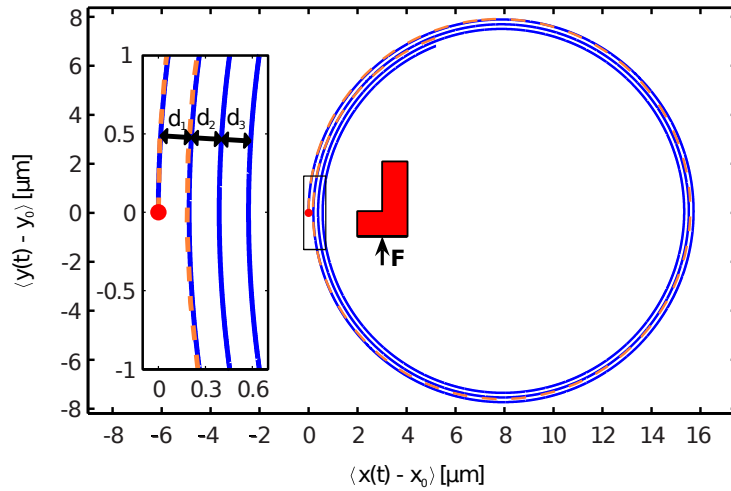

Fig. 5: *Noise-averaged trajectory of a Brownian circle swimmer for a prescribed position and orientation at $t = 0$. The dashed curve is the experimental one obtained for a chiral L-shaped colloidal model swimmer. The solid curve shows the theoretical prediction of the spira mirabilis with the starting point indicated by a red bullet. Inset: close-up of the framed area in the plot. As a characteristic feature of the logarithmic spiral, the ratio d_{i+1}/d_i of the distances d_i between adjacent turns of the mean swimming path are constant. From Ref. [20].*

Finally, in three dimensions, the noise-averaged trajectory is a concho-spiral [30] which is a generalization of the logarithmic spiral.

3.2   Circle swimmers in gravity

The motion of circle swimmer in an external gravitational field has been studied by experiments and theory by using L-shaped articial swimmers on a tilted two-dimensional substrate. Interesting a situation of negative gravitaxis was found where the chiral self-propelled particles swims against gravity [31]. The physical origin is a balance of torques which arise from the self-propulsion and from gravity. The resulting motion is linear. This mechanism does only occur for chiral anisotropic particles and is different from bottom-heaviness [32] which is another reason for negative gravitaxis.

4   Bacterial turbulence

4.1   The bulk state of active turbulence

Based on a self-propelled rod model of linear swimmers, the emerging state diagram was explored by Wensink and coworkers [33, 34] as a function of two parameters, namely the area fraction ϕ and the aspect ratio of the rods. The temperature was set to zero and the strength of the self-propelling force relative to the repulsive interaction was kept fixed. The simulations were performed in two spatial dimensions. In the two-dimensional parameter space, a rich state diagram was found which is shown in figure 6.
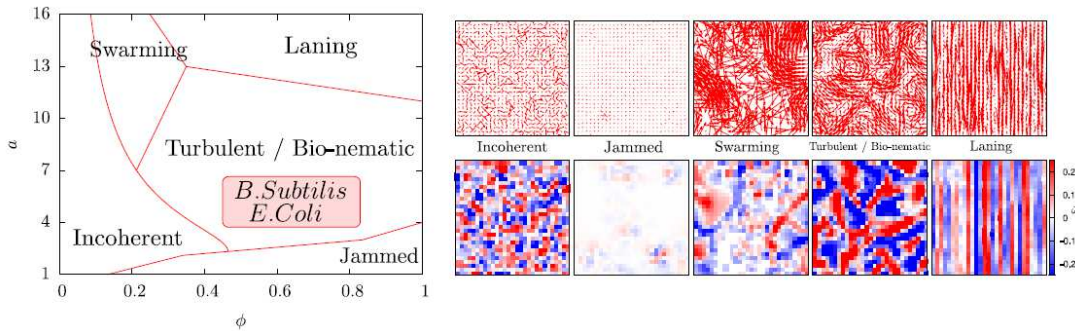

Fig. 6: *Schematic non-equilibrium phase diagram of the 2D SPR model at variable aspect ratio a and effective density ϕ. The area relevant to self-motile bacteria is highlighted in red. A number of distinctly different dynamical states are discernible as indicated by the coarse-grained maps of the velocity field $\vec{v}(\vec{r}, t)$ (upper panels) at time t and the corresponding scalar vorticity field $\tilde{\omega}(\vec{r}, t) = [\nabla \times \vec{v}(\vec{r}, t)] \cdot \hat{e}_z$ expressed in units of τ_0^{-1}. From Ref. [34].*

For small densities, obviously a dilute phase is found which lacks any significant swarming. For higher densities and large aspect ratios, a swarming state occurs where large clusters are formed by aligning interactions and self-propulsion. This swarming state shows the characteristics of large density fluctuations. For small aspect ratios, on the other hand, there is a jammed state at high densities. Exactly at aspect ratio of 1 (spherical particles) an active crystal is formed [35, 36]. For both high density and high aspect ratio, a lane phase occurs as in driven passive systems [37, 38]. Interesting and novel behaviour is visible for intermediate parameters, there is a bionematic and a "turbulent" state. The former state is mainly characterized by nematic ordering while the latter possesses a significant degree of swirling. Though a bit arbitrary, the distinction between bionematic and turbulent state can be done via the behaviour of the equal-time autocorrelation function of the coarse-grained velocity field $\vec{v}(\vec{r}, t)$ as a function of distance

r: If it crosses zero at a certain distance $r = R$ this marks the radius R of a typical swirl and the state is called "turbulent" if it does not cross zero, it is called "bionematic". Such a velocity correlation function is shown in figure 7.
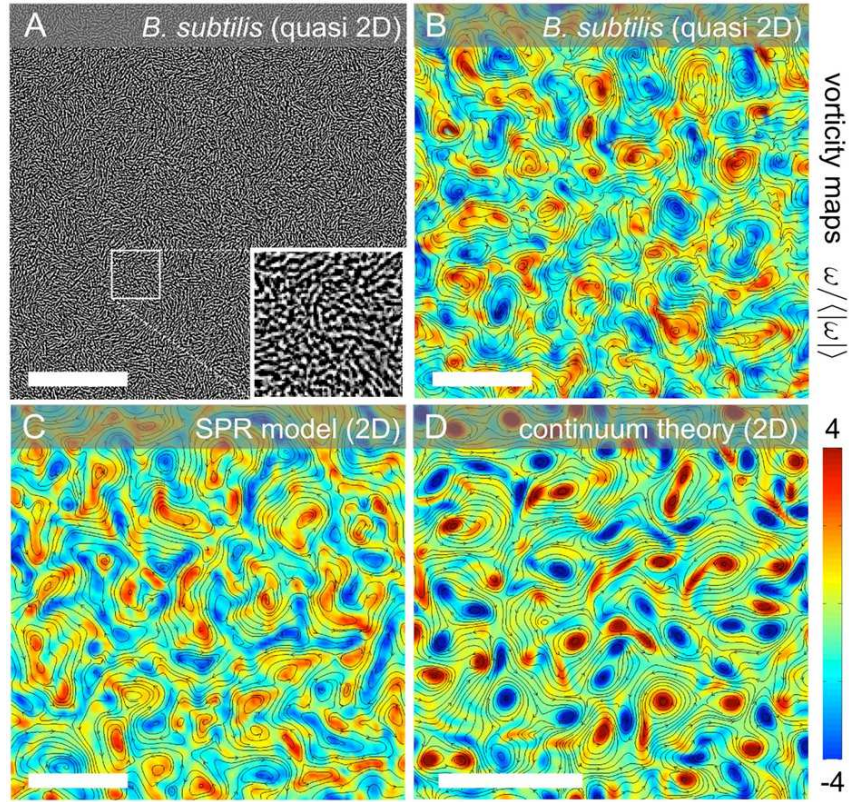

Fig. 7: *Experimental snapshot (A) of a highly concentrated, homogeneous quasi-2D bacterial suspension. Flow streamlines $\mathrm{v}(t, \vec{r})$ and vorticity fields $\omega(t, \vec{r})$ in the turbulent regime, as obtained from (B) quasi-2D bacteria experiments, (C) simulations of the deterministic SPR model ($a = 5$; $\phi = 0.84$), and (D) continuum theory. The range of the simulation data in D was adapted to the experimental field of view ($217\mu m \times 217\mu m$) by matching the typical vortex size (Scale bars, 50 μm). From Ref. [33].*

The turbulent state occurs at aspect ratios which are typical for real bacteria such as E. coli or bacillus subtilis. Indeed experiments on strongly confined bacteria have confirmed the occurence of a turbulent state. The enstrophy Ω of a coarse-grained velocity field of the swimmers is another more sensible order parameter for the "turbulent" state. It is defined as

$$\Omega = \frac{1}{2}\langle |\widetilde{\omega(\vec{r}, t)}|^2 \rangle \tag{15}$$

with $\omega(\vec{r}, t) = [\nabla \times \vec{v}(\vec{r}, t)] \cdot \hat{\mathrm{e}}_z$ and the tilde means a spatial average. In the turbulent state, the averaged chirality is zero. Still there is a significant local chirality as revealed by the strong peaks in the vorticity of the coarse-grained velocity field, see figure 6. A significant degree of swirling is visible there. There is also a characteristic extension of the swirls which is about 30 larger than the size of the self-propelled rods. Moreover in figure 7 experimental data for bacillus subtilis suspensions in the turbulent state and results from an extension of the Toner-Tu model of active nematics which includes a gradient expansion are shown. More details about the theory can be found in Refs. [33, 39].
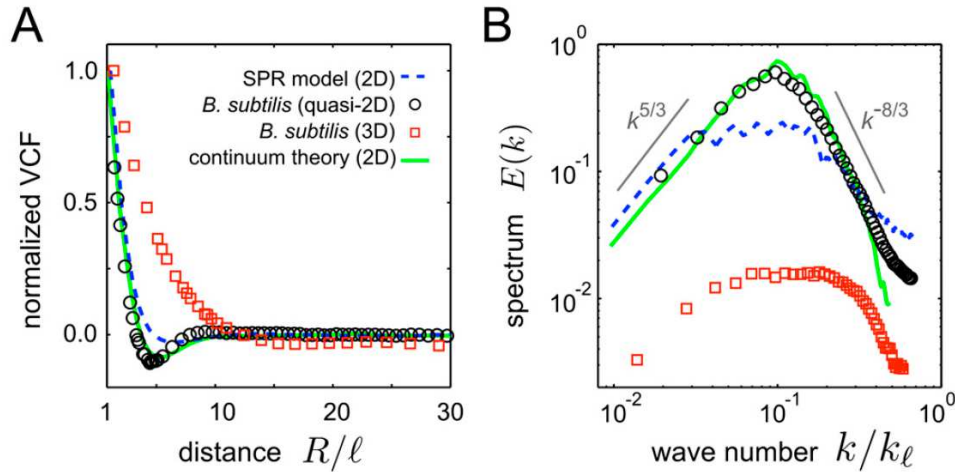
Fig. 8: *Equal-time velocity correlation functions (VCFs), normalized to unity at $R = \ell$, and flow spectra for the two-dimensional self-propelled-rod model, B. subtilis experiments, and 2D continuum theory. (A) The minima of the VCFs reflect the characteristic vortex size R_v. Data points present averages over all directions and time steps to maximize sample size. (B) For bulk turbulence (red squares) the 3D spectrum is plotted ($k_\ell = 2\pi/\ell$), the other curves show 2D spectra. Spectra for the 2D continuum theory and quasi-2D experimental data are in good agreement; those of the 2D SPR model and the 3D bacterial data show similar asymptotic scaling but exhibit an intermediate plateau region (spectra multiplied by constants for better visibility and comparison). From Ref. [33].*

It is important to note that in many occasions the term turbulence is reserved for fluid motion at high Reynolds number complementary to the present situation which happens at low Reynolds number. However, the Greek work "$\tau \upsilon \rho \beta \eta$" from which the word turbulence roots means perturbation or swirling in a quite general sense. Therefore the term "turbulence" can be used in a more general way. In order to avoid confusion, the term "active turbulence" [40] or "**bacterial turbulence**" [39] has been introduced which delineates the effect considered here from high-Reynolds number turbulence. Another term which has been used is "mesoscale turbulence" [33] which stresses the fact that there is a maximal swirl size which is also different to traditional turbulence where swirls occur on all scales.

Finally the scaling of the energy spectrum has been explored as well. An interesting question is whether the traditional Kolmogorow-Kraichnan scaling of high-Reynolds-number turbulence is valid. This would be a power-law decay in the inertial regime where the energy spectrum

$$E(k) \sim k \int d\vec{r}\exp[i\vec{k} \cdot \vec{r}]\langle \vec{v}(t, 0) \cdot \vec{v}(t, \vec{r})\rangle_t \tag{16}$$

scales with the wave number k as $k^{-5/3}$. In fact this exponent is not found in bacterial turbulence (see figure 8) where rather an exponent $-8/3$ shows up in the limited scaling window. Therefore bacterial turbulence is qualitatively different from ordinary turbulence at high Reynolds numbers. It is still unclear since the scaling regime is limited by the typical inverse swirl size whether the found exponent is universal or whether it is nonuniversal or just a crossover. More evidence for a true scaling has been obtained in the opposite limit of small wave numbers k. Here recent studies [41] have found that there is another scaling limit characterized by a nonuniversal exponent which can be in general different to the one occuring in the Kolmogorov-Kraichnan

scaling. This nicely demonstrates that bacterial turbulence is a complex phenomenon which lacks universal scaling.

4.2   What can we do with bacterial turbulence?

After we have clarified the occurence of bacterial turbulence in the bulk (in two spatial dimensions), we now turn to the effect of boundaries of bacterial turbulence. The understanding of this leads to important applications such as the motion of passive objects in a turbulent bath. An important feature found in Ref. [42] is that a hard boundary just suppresses the occurence of swirls. This leads directly to a depletion of swirls in a cuspy environment which has important consequences.

a) Single carrier

A standard example of a nontrivial nonlinear geometry is a wegde-like carrier (a V-shaped passive particle). Let us assume that the size of the carrier is comparable to the typical swirl size R. Then there is an important difference between the inside and the outside region of the carrier as far as the occurence of swirls is concerned which is illustrated in figure 9.
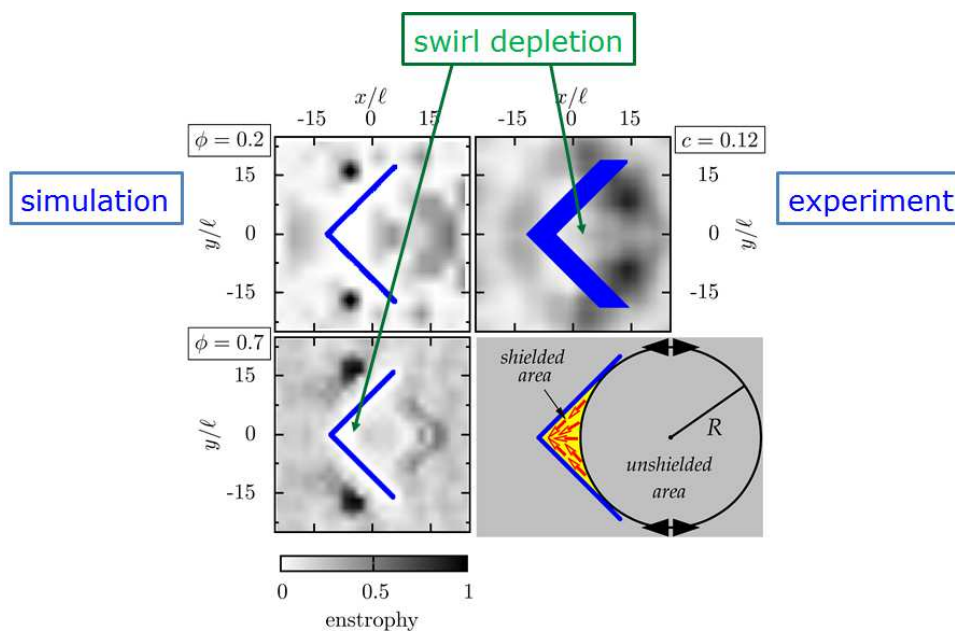

Fig. 9: *Normalized local magnitude of vorticity obtained from simulations (left column) and experiment (top right). Bottom right: Illustration of swirl shielding in the carrier cusp. Bacteria in the shielded area (light colored) are indicated by arrows and the unshielded area is marked by dark color. The typical swirl radius R for different bacteria concentrations is obtained as the first minimum of the equal-time spatial velocity autocorrelation function. From Ref. [42].*

The outside does not put any constraint for a full swirl while the inside when narrow enough excludes full swirls. Hence we expect a depletion of swirls inside close to the cusp which results in an area shielded from swirks. This is in fact confirmed by computer simulation of the self-propelled rod model. The swirl depletion induces a translational motion of the carrier along its cusp. At the inner wedge cusp, rods are accumulating which are pushing the carrier. As these are shielded from swirls, they provide an efficient and powerful driving

source of the carrier such that the bacterial-induced velocity of the carrier is optimized in the turbulent bulk phase of the rods.

b) Two carriers

When an active bath is exposed to two carriers fixed in their relative orientation, swirl depletion again plays the key role in driving their joint motion. There is a depletion attraction between neighbouring rods driving them together and ultimately leading to stacking of the carriers. This is demonstrated in figure 10.
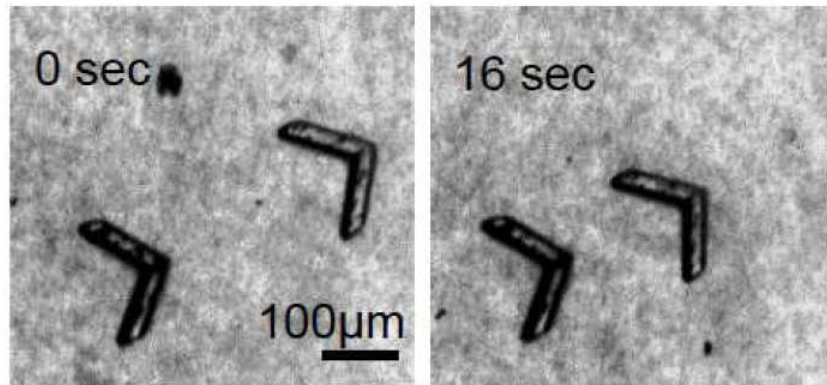

Fig. 10: *Illustration of the attraction of wedge-like carriers in a turbulent bacterial bath. The two wedges approach each other as a function of time. From Ref. [43]*

Of course, many carriers are expected to pile up in long stacks similar to the behaviour of colloidal bowls [44].

c) Other effects

The occurence of bacterial turbulence was explored in the presence of many passive particles which were strongly interacting thus forming a stable network which a tunable spacing. Experiments and computer simulations [45, 46] have shown that turbulence is suppressed if the characteristic spacing between the passive particles becomes comparable to the swirl size. This demonstrates that bacterial turbulence can be tailored at wish by using passive particles as obstacles and gives a first insight about bacterial turbulence in heterogeneous media (such as porous materials).

For mobile and weakly interacting passive particles, on the other hand, one can expect on the grounds of swirl depletion that a phase separation between the passive particles occurs as induced by turbulence. However, this expectation still needs to be verified.

5   Conclusions

We have considered recent aspects of chiral circling motion of microswimmers. First we studied active Brownian motion of a single circle swimmer. In this case the circular motion is induced by an intrinsic left-right asymmetry of the swimmer. Then we have considered the collective motion of linear swimmers where large swirls are emerging due to excluded volume interactions and self-propulsion. There will be number of future problems which will be explored soon in

this rapidly developing field. We are just at the beginning to understand the collective behaviour of many circle swimmers [47] which may form vortex pairs. Moreover the universality of bacterial turbulence needs to be explored more. It would be interesting to confirm a turbulent state also in suspensions of rod-like artificial microswimmers.

References

[1] H. S. Jennings. On the significance of the the spiral swimming of organisms. *Amer. Soc. Natural.*, 35:369, 1901.

[2] H. C. Berg and L. Turner. Chemotaxis of bacteria in glass-capillary arrays - escherichia-coli, motility, microchannel plate, and light-scattering. *Biophys. J.*, 58:919, 1990.

[3] W. R. DiLuzio, L. Turner, M. Mayer, P. Garstecki, D. B. Weibel, H. C. Berg, and G. M. Whitesides. *Escherichia coli* swim on the right-hand side. *Nature*, 435:12714, 2005.

[4] E. Lauga, W. R. DiLuzio, G. M. Whitesides, and H. A. Stone. Swimming in circles: Motion of bacteria near solid boundaries. *Biophys. J.*, 90:400, 2006.

[5] J. Hill, O. Kalkanci, J. L. McMurry, and H. Koser. Hydrodynamic surface interactions enable escherichia coli to seek efficient routes to swim upstream. *Phys. Rev. Lett.*, 98:068101, 2007.

[6] V. B. Shenoy, D. T. Tambe, A. Prasad, and J. A. Theriot. A kinematic description of the trajectories of listeria monocytogenes propelled by actin comet tails. *PNAS*, 104:8229, 2007.

[7] S. Schmidt, J. van der Gucht, P. M. Biesheuvel, R. Weinkamer, E. Helfer, and A. Fery. Non-Gaussian curvature distribution of actin-propelled biomimetic colloid trajectories. *Eur. Biophys. J.*, 37:1361, 2008.

[8] I. H. Riedel, K. Kruse, and J. Howard. A self-organized vortex array of hydrodynamically entrained sperm cells. *Science*, 309:300, 2005.

[9] D. M. Woolley. Motility of spermatozoa at surfaces. *Reproduction*, 126:259, 2003.

[10] B. M. Friedrich and F. Jülicher. The stochastic dance of circling sperm cells: sperm chemotaxis in the plane. *New J. Phys.*, 10:123025, 2008.

[11] G. Corkidi, B. Taboada, C. D. Wood, A. Guerrero, and A. Darszon. Tracking sperm in three-dimensions. *Biochem. Biophys. Res. Commun.*, 373:125, 2008.

[12] C. J. Brokaw. Chemotaxis of bracken spermatozoids - the role of bimalate ions. *J. Exp. Biol.*, 35(1):192, 1958.

[13] C. J. Brokaw. Random and oriented movements of bracken spermatozoids. *J. Cell. Comp. Physiol.*, 54:95, 1959.

[14] H. C. Crenshaw. A new look at locomotion in microorganisms: Rotating and translating. *American Zoologist*, 36:608, 1996.

[15] T. Fenchel and N. Blackburn. Motile chemosensory behaviour of phagotrophic protists: Mechanisms for and efficiency in congregating at food patches. *Protist*, 150:325, 1999.

[16] M. J. McHenry and J. A. Strother. The kinematics of phototaxis in larvae of the ascidian aplidium constellatum. *Marine Biology*, 142:173, 2003.

[17] G. Jékely, J. Colombelli, H. Hausen, K. Guy, E. Stelzer, F. Nédélec, and D. Arendt. Mechanism of phototaxis in marine zooplankton. *Nature*, 456:395, 2008.

[18] R. Thar and T. Fenchel. True chemotaxis in oxygen gradients of the sulfur-oxidizing bacterium thiovulum majus. *Appl. Environ. Microbiol.*, 67:3299, 2001.

[19] S. Nakata, Y. Iguchi, S. Ose, M. Kuboyama, T. Ishii, and K. Yoshikawa. Self-rotation of a camphor scraping on water: New insight into the old problem. *Langmuir*, 13:4454, 1997.

[20] F. Kümmel, B. ten Hagen, R. Wittkowski, I. Buttinoni, R. Eichhorn, G. Volpe, H. Löwen, and C. Bechinger. Circular motion of asymmetric self-propelling particles. *Phys. Rev. Lett.*, 110:198302, 2013.

[21] T. Ohta and T. Ohkuma. Deformable self-propelled particles. *Phys. Rev. Lett.*, 102:154101, 2009.

[22] T. Obata, T. Shimizu, H. Osaki, H. Oshima, and H. Hara. Fluctuations in human's walking (ii). *J. Korean Phys. Soc.*, 46:713, 2005.

[23] D. J. Kraft, R. Wittkowski, B. ten Hagen, K. V. Edmond, D. J. Pine, and H. Löwen. Brownian motion and the hydrodynamic friction matrix for colloidal particles of complex shape. *Phys. Rev. E*, 88:050301(R), 2013.

[24] G. S. Redner, A. Baskaran, and M. F. Hagan. Reentrant phase behavior in active colloids with attraction. *Phys. Rev. E*, 88:012305, 2013.

[25] I. Buttinoni, J. Bialke, F. Kümmel, H. Lwen, C. Bechinger, and T. Speck. Dynamical clustering and phase separation in suspensions of self-propelled colloidal particles. *Phys. Rev. Lett.*, 110:238301, 2013.

[26] A. Kaiser, K. Popowa, and H. Löwen. Active dipole clusters: from helical motion to fission, 2015. arXiv:1503.03315.

[27] A. Cēbers. Diffusion of magnetotactic bacterium in rotating magnetic field. *J. Magn. Magn. Mater.*, 323:279, 2011.

[28] S. van Teeffelen and H. Löwen. Dynamics of a Brownian circle swimmer. *Phys. Rev. E*, 78:020101(R), 2008.

[29] J. R. Howse, R. A. L. Jones, A. J. Ryan, T. Gough, R. Vafabakhsh, and R. Golestanian. Self-motile colloidal particles: From directed propulsion to random walk. *Phys. Rev. Lett.*, 99:048102, 2007.

[30] R. Wittkowski and H. Löwen. Self-propelled Brownian spinning top: dynamics of a biaxial swimmer at low Reynolds numbers. *Phys. Rev. E*, 85:021406, 2012.

[31] B. ten Hagen, F. Kümmel, R. Wittkowski, D. Takagi, H. Löwen, and C. Bechinger. Gravitaxis of asymmetric self-propelled colloidal particles. *Nature Communications*, 5:4829, 2014.

[32] K. Wolff, A. M. Hahn, and H. Stark. Sedimentation and polar order of active bottom-heavy particles. *Eur. Phys. J. E*, 36:43, 2013.

[33] H. H. Wensink, J. Dunkel, S. Heidenreich, K. Drescher, R. E. Goldstein, H. Löwen, and J. M. Yeomans. Meso-scale turbulence in living fluids. *PNAS*, 109:14308, 2012.

[34] H. H. Wensink and H. Löwen. Emergent states in dense systems of active rods: from swarming to turbulence. *J. Phys.: Condens. Matter*, 24:464130, 2012.

[35] J. Bialké, T. Speck, and H. Löwen. Crystallization in a dense suspension of self-propelled particles. *Phys. Rev. Lett.*, 108:168301, 2012.

[36] A. M. Menzel and H. Löwen. Traveling and resting crystals in active systems. *Phys. Rev. Lett.*, 110:055702, 2013.

[37] J. Dzubiella, G. P. Hoffmann, and H. Löwen. Lane formation in colloidal mixtures driven by an external field. *Phys. Rev. E*, 65:021402, 2002.

[38] T. Vissers, A. Wysocki, M. Rex, H. Löwen, C. P. Royall, and A. Imhof, A. van Blaaderen. Lane formation in driven mixtures of oppositely charged colloids. *Soft Matter*, 7:2352, 2011.

[39] J. Dunkel, S. Heidenreich, K. Drescher, H. H. Wensink, M. Br, and R. E. Goldstein. Fluid dynamics of bacterial turbulence. *Phys. Rev. Lett.*, 110:228102, 2013.

[40] J. M. Yeomans. Active matter: Playful topology. *Nature Materials*, 13:1004, 2014.

[41] D. Grošelj, F. Jenko, and E. Frey. How turbulence regulates biodiversity in systems with cyclic competition. *Phys. Rev. E*, 91:033009, 2015.

[42] A. Kaiser, A. Peshkow, A. Sokolov, B. ten Hagen, H. Löwen, and I. S. Aranson. Transport powered by bacterial turbulence. *Phys. Rev. Letters*, 112:158101, 2014.

[43] A. Kaiser, A. Sokolov, I. S. Aranson, and H. Löwen. Motion of two micro-wedges in a turbulent bacterial bath. *European Physical Journal: Special Topics*, accepted, 2015.

[44] M. Marechal, R. J. Kortschot, A. F. Demirörs, A. Imhof, and M. Dijkstra. Phase behavior and structure of a new colloidal model system of bowl-shaped particles. *Nano Lett.*, 10:1907, 2010.

[45] K.-A. Liu and L. I. Multifractal dynamics of turbulent flows in swimming bacterial suspensions. *Phys. Rev. E*, 86:011924, 2012.

[46] Y.-S. Su, H.-C. Wang, and L. I. Suppressing turbulence of self-propelling rods by strongly coupled passive particles. *Phys. Rev. E*, 91:030302(R), 2015.

[47] A. Kaiser and H. Löwen. Vortex arrays as emergent collective phenomena for circle swimmers. *Phys. Rev. E*, 87:032712, 2013.